Available online at www.sciencedirect.com
ScienceDirect
Journal of Power Sources 167 (2007) 398–405
JOURNAL OF POWER SOURCES
www.elsevier.com/locate/jpowsour

3-D model of thermo-fluid and electrochemical for planar SOFC

Guilan Wang [a], Yunzhen Yang [a,*], Haiou Zhang [b], Weisheng Xia [a]

[a] State Key Laboratory of Material Processing and Die and Mould Technology, Huazhong University of Science and Technology, Wuhan 430074, PR China
[b] State Key Laboratory of Digital Manufacturing Equipment and Technology, Huazhong University of Science and Technology, Wuhan 430074, PR China

Received 25 December 2006; received in revised form 9 February 2007; accepted 9 February 2007
Available online 25 February 2007

Abstract

A numerical simulation tool for calculating the planar solid oxide fuel cells was described. The finite volume method was employed for the simulation, which was on the basis of the fundamental conservation laws of mass, momentum, energy and electrical charge. Temperature distributions, molar concentrations of gaseous species, current density and over potential were calculated using a single cell unit model with double channels of co-flow and counter-flow cases. The influences of operating conditions and anode structure on the performances of SOFC were also discussed. Simulation results show that the co-flow case has more uniform temperature and current density distributions and smaller temperature gradients, thus offers thermostructural advantages than the counter-flow case. Moreover, in co-flow case, with the increasing of delivery rate, temperature and hydrogen mass fraction of fuel, average temperature of PEN, current density and activation potential also rise. However, with increasing the delivery rate of air, average temperature of PEN decreases. In particular, it is effective to improve the output voltage by reducing the thickness of anode or increasing its porosity.

Keywords: Planar SOFC; Thermo-fluid model; Electrochemical model; Temperature field; Current density; Over potential

1. Introduction

The solid oxide fuel cell (SOFC) has been drawn attention because of its higher energy conversion efficiency, power density, low environmental hazards and production cost. Thus, the SOFC is expected to reach commercialization in a few years and could be a promising alternative energy source for residential and distributed power plants in the 21st century [1–3]. However, further development of the planar SOFC faces challenges related to maximizing the power density and minimizing the non-uniform distribution of temperature, which contributes to thermal stress in the SOFC components [4–5].

The temperature and current density distributions in a SOFC are determined by the working conditions, such as the delivery rates and temperatures of the fuel and air to the system. Fuel utilization and fuel distribution are also critical due to the exothermic electrochemical reactions. Increased fuel flow tends to increase the uniformity of the reaction rates across the active area and decrease fuel utilization. Decreased fuel flow tends to increase the fuel utilization, but can cause local fuel depletion and cold spots that exacerbate temperature non-uniformities. Air and fuel inlet temperatures also affect the reaction rates, cell temperature and fuel utilization. Therefore, management of the flow of air and fuel and the distribution of each, is critical to the stable operation of the cell [5]. Other factors that affect the temperature distribution and fuel utilization are the thickness and porosity of the anode. As a consequence, the geometrical design of SOFC is important in establishing a well-operating cell. In order to efficiently develop planar SOFC stacks, it is convenient and effective to have the capability to experiment numerically with the effects of different geometric designs on the operation and performance.

In the past, modeling of the planar SOFC during steady operation to calculate the temperature and current density distributions has been reported [6–12]. Investigations of planar SOFC operation and planar SOFC performance have predicted cell temperature and current distribution for various flow patterns [13–14]. However, only less work has been performed on the influences of variation of structure and operating conditions on the performance of SOFCs [15]. The purpose of present work is to demonstrate a model to predict temperature distributions, species concentrations, current density and

* Corresponding author. Tel.: +86 27 62475231; fax: +86 27 87557394.
E-mail address: ch9998@zzu.edu.cn (Y. Yang).

0378-7753/$ – see front matter © 2007 Elsevier B.V. All rights reserved.
doi:10.1016/j.jpowsour.2007.02.019

Nomenclature

C_k	concentration of component k
C_p	specific heat (J kg^{-1} K^{-1})
$D_{k,eff}$	effect diffusivity of component k (m^2 s^{-1})
E_f	internal energy of mixture gas (J)
E_s	internal energy of solid (J)
F	Faraday constant (C mol^{-1})
I	local current density (A/cm^2)
I_k	mass source of mixture component k
j	transfer current density (A cm^2)
k_{eff}	effect thermal conductivity coefficient (W m^{-1})
k_f	thermal conductivity coefficient of gas (W m^{-1})
k_s	thermal conductivity coefficient of solid (Wm^{-1})
K	permeability coefficient (m^2)
P	pressure of mixture (Pa)
R	gas constant (J mol^{-1} K^{-1})
s_k	reaction coefficient of component k
S_E	energy source (J)
S_M	momentum source
ΔS	entropy change (J mol^{-1})
T	Temperature (K)
U	mixture velocity (m/s)

Greek letters

δ	anode thickness (m)
ε	porosity
$\eta_{act,a}$	activation potential at anode (V)
$\eta_{act,c}$	activation potential at cathode (V)
η_{conc}	concentration potential (V)
μ_{eff}	effect viscosity
ρ	density (kg m^{-3})
σ_{eff}	effect electrical conductivity (Ω^{-1} m^{-1})

over potentials. In this study, co- and cross-flow cases were examined. In particular, the effects of the structural parameters and the operating conditions on the performance of a SOFC are discussed in a co-flow case, such as thickness and porosity of anode, delivery rates and temperatures of fuel and air.

2. Mathematics model

2.1. Model geometry

Generally, the repeating unit of a typical planar SOFC stack is constructed of a positive electrode–electrolyte–negative electrode (PEN) and an interconnector plate "stacked" together. For the sake of simplicity of calculation, one repeating cell unit, which includes a PEN, air and fuel channels and 1/2 interconnect thickness top and bottom in the *Y*-direction, was analyzed in this simulation. The one-cell stack and the single unit model are illustrated in Fig. 1. In this model, the thicknesses of anode, cathode, electrolyte and interconnect were 0.5, 0.25, 0.05 and 1.0 mm, respectively.

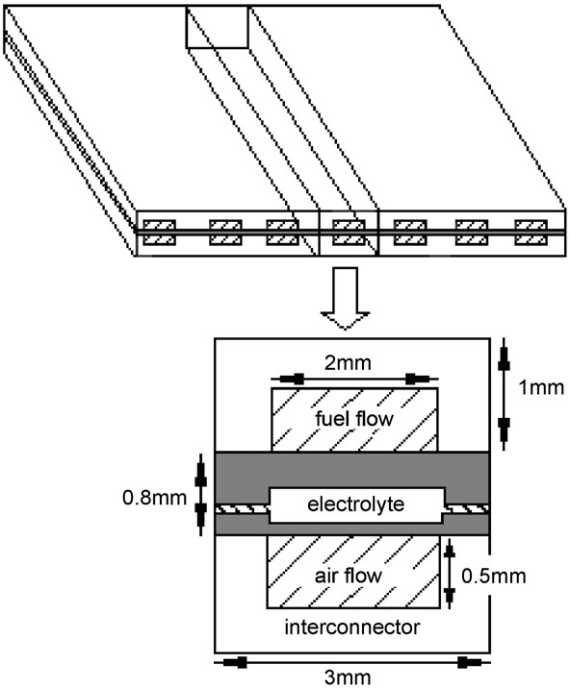

Fig. 1. Illustrations of the one cell-stack and singe cell unit model.

2.2. Thermo-fluid model

The ANSYS-CFX code was selected to solve the thermo-fluid model. In the simulation, the solid and fluid domains were divided into some discrete meshes, and in each computational mesh, the conservation equations of species, mass, momentum and energy were solved using the finite volume method.

In general, gas species transfer mainly by convection in the flow channels and diffusion in the porous electrodes. The species conservation equation:

$$\nabla(\rho C_k U) = \nabla(D_{k,eff}\nabla C_k) + I_k, \quad k = H_2, O_2, H_2O \tag{1}$$

where I_k is the rate of production or consumption of specie k, and given by [16]:

$$I_k = \pm\frac{s_k j}{2F} \tag{2}$$

The diffusion coefficients of hydrogen and oxygen are obtained as follow [16]:

$$D_{O_2} = 0.181 \times \left(\frac{T}{273}\right)^{1.5}, \qquad D_{H_2} = 0.753 \times \left(\frac{T}{273}\right)^{1.5} \tag{3}$$

The mass conservation equation:

$$\nabla \cdot (\varepsilon\rho U) = 0 \tag{4}$$

Both the air and fuel flows were considered as ideal gas mixtures with the density given by:

$$\rho = \frac{P}{RT}\left(\sum_k \frac{m_k}{M_k}\right) \tag{5}$$

where m_k is the mass fraction of specie k with molecular weight M_k.

The momentum conservation equation:

$$\rho\varepsilon\left(u\frac{\partial u}{\partial x}+v\frac{\partial v}{\partial y}+w\frac{\partial w}{\partial z}\right) = -\varepsilon\nabla P+\varepsilon\mu_{\text{eff}}\left(\frac{\partial u^2}{\partial x^2}+\frac{\partial v^2}{\partial y^2}+\frac{\partial w^2}{\partial z^2}\right)+S_M \quad (6)$$

where S_M is momentum source, and $S_M=0$ in the flow channels. However, in the porous electrodes, Darcy law with constant porosity and permeability is applied to model the momentum source as follows [16]:

$$S_M=-\frac{\mu_{\text{eff}}}{K}\varepsilon^2 U \quad (7)$$

where u_{eff} is the effective viscosity of the mixture gas and is given by [16]:

$$\mu_{\text{eff}}=\sum_k\frac{X_k\mu_k}{\sum_k X_k\phi_{kj}} \quad (8)$$

$$\phi_{kl}=\frac{\left[1+(\mu_k/\mu_j)^{1/2}(M_j/M_k)^{1/4}\right]^2}{\left[8(1+(M_k/M_j))\right]^{1/2}} \quad (9)$$

where X_k is the molar percent of the specie k, μ_j and μ_k are kinematical viscosities of specie j and k, respectively.

The energy conservation equation

$$\nabla\cdot(U(\rho_f E_f+p))+\nabla\cdot(\tau U)+\nabla\cdot(k_{\text{eff}}\nabla T)+S_E=0 \quad (10)$$

Heat transfer between the fluid and solid materials was limited to conduction and convection, and the effect of radiation was neglected in this calculation because it is very small relative to the other kinds of heat transfer. Additionally, the effective thermal conductivities of porous electrodes are calculated by the following Eq. (11) [17]:

$$k_{\text{eff}}=\varepsilon k_f+(1-\varepsilon)k_s \quad (11)$$

where k_f and k_s are thermal conductivities of fluid and solid, respectively. S_E is energy source term expressed by Eq. (12) and mainly consists of reaction and Ohmic heats [16].

$$S_E=\frac{i^2}{\sigma_{\text{eff}}}+\frac{i}{\delta}\left(\frac{T\Delta S}{2F}+\eta_{\text{act}}\right) \quad (12)$$

Specific heats of gas components are described as the functions of temperature [16]:

$$C_p=a+b\times10^3T+c\times10^6T^2 \quad (13)$$

Table 1
Coefficients of the specific heats of gas

Gas	*a*	*b*	*c*
Hydrogen	25.8911	−0.8373	2.0138
Oxide	29.0856	12.9874	−3.8644
Water gas	30.3794	9.6212	1.1848

where *a*, *b* and *c* are relevant coefficients, as listed in Table 1. Solid material properties used in this simulation are listed in Table 2.

2.3. Boundary conditions

The cell unit considered in this simulation represented a repeating unit in the middle of a large stack, and external walls of the cell unit were assumed to be adiabatic. Constant temperature, delivery rate, and gaseous composition were imposed at the inlet boundaries for the fuel and air.

2.4. Electrochemical model

2.4.1. Assumptions and reactions

The oxidant reduction reaction occurring at the cathode is expressed as follows:

$$\tfrac{1}{2}O_2+2e^-\rightarrow O^{2-} \quad (14)$$

The oxygen ions transfer through the electrolyte and then into the active reaction areas of anode. The electrochemical reaction of fuel at the anode is:

$$H_2+O^{2-}\rightarrow H_2O+2e^- \quad (15)$$

So the overall reaction is:

$$H_2+\tfrac{1}{2}O_2\rightarrow H_2O \quad (16)$$

2.4.2. Dynamics of electrochemical reactions

According to Faraday's law, the reaction rates depend on the current density *i* [7]:

$$i=2F\frac{df}{dt}=4F\frac{dO_2}{dt} \quad (17)$$

where df/dt, dO_2/dt are the molar consumption rates of fuel and oxygen at the anode and the cathode, respectively.

During the process of energy transforming, when the charge transfer reaction at the electrolyte–electrode interface is too slow to provide ions at the rate required by the demand of current,

Table 2
Properties of the solid material

Cell component	Density	Effect thermal conductivity (W/m K)	Specific heat (J/kg K)	Porosity (%)	Permeability coefficient (m^2)
Interconnect	7700	13	0.8	–	–
Anode	6200	6.23	0.65	25/35/45	1.0E−12
Cathode	6000	9.6	0.9	35	1.0E−12
Electrolyte	5560	2.7	0.3	–	–

the activation polarization occurs and is defined by the Butler-Volmer equation [18]:

$$i = i_0 \left\{ \exp\left(-\beta \frac{2F}{RT}\eta_{\text{act}}\right) - \left(\exp(1-\beta)\frac{2F}{RT}\eta_{\text{act}}\right)\right\} \quad (18)$$

Eq. (18) is simplified and described by the Tafel empirical formula [18,19]:

$$\eta_{\text{act,a}} = \frac{RT}{2Fi_{0,\text{a}}} i \quad (19)$$

$$\eta_{\text{act,c}} = -\left(\frac{RT}{2\beta F}\right)\ln i_{0,\text{c}} + \left(\frac{RT}{2\beta F}\right)\ln i \quad (20)$$

where β is the transmission coefficient and $\beta = 0.5$ in this simulation, $\eta_{\text{act,a}}$ and $\eta_{\text{act,c}}$ are the activation potentials at the anode and the cathode, respectively. $i_{0,\text{a}}$ and $i_{0,\text{c}}$ are the exchange current densities at the anode and the cathode, respectively. In this study, exchange current densities at the anode and the cathode are 5300 and 2300 A/cm^2, respectively.

The concentration polarization is also calculated as follows [18]:

$$\eta_{\text{con}} = -\frac{RT}{2F}\ln\left[\frac{y_{\text{H}_2,\text{A/E}}\, y_{\text{H}_2\text{O,bulk}}}{y_{\text{H}_2,\text{bulk}}\, y_{\text{H}_2\text{O,A/E}}}\right] \quad (21)$$

where $y_{\text{H}_2,\text{bulk}}$ and $y_{\text{H}_2\text{O,bulk}}$ are the hydrogen and water gas molar fractions in the fuel flow channel, respectively. $y_{\text{H}_2,\text{A/E}}$ and $y_{\text{H}_2,\text{A/E}}$ are those in the interface of electrolyte/anode, respectively.

Ohmic polarization is ignored in this simulation, so the open-circuit voltage is given by:

$$V = E - \eta_{\text{act}} - \eta_{\text{con}} \quad (22)$$

where V is the open-circuit voltage and E is Nernst voltage obtained by:

$$E = \frac{RT}{2F}\ln K + \frac{RT}{2F}\ln\left[\frac{(p_{\text{H}_2}) \times (p_{\text{O}_2})^{1/2}}{(p_{\text{H}_2\text{O}})}\right] \quad (23)$$

where E_0 is the standard voltage of the cell, $p_{\text{H}_2\text{O}}$, p_{O_2} and p_{H_2} are the partial pressures of water gas, oxygen and hydrogen, respectively.

3. Simulation results and discussion

In the calculations, the modeling tool couples an electrochemical calculation method with a commercial computational fluid dynamics (CFD) simulation code. The finite-volume Navier–Stokes and transport equations are solved to obtain the gas species concentrations and temperatures at each position in the cell. The information is passed to the electrochemical model (subroutine). Then the local current density is calculated and applied to obtain the hydrogen reaction rate, heat source and species sources. Gas species concentrations and temperature distributions are then calculated for the next iteration, and so on, until convergence of solution is achieved. The cell operating conditions used for the simulation are listed in Table 3.

Fig. 2 presents the temperature distributions of PEN for co-flow case and counter-flow case under the first working conditions. The average temperature of PEN is 979 °C with maximum and minimum temperatures of 1053 and 916 °C in co-flow case. Furthermore, it can be seen that the temperature of PEN increases uniformly along the direction of fuel flow, and is highest near the fuel outlet. However, for counter-flow case, average temperature is 996 °C with maximum and minimum temperatures of 1088 and 923 °C. In addition, it should be noted that the temperature of the PEN rises rapidly, reaching a maximum near the fuel inlet, and then gradually drops. Of the two flow configurations calculated, the co-flow case has the more uniform temperature distribution and a smaller temperature difference (ΔT) from the air inlet to the outlet. This is due to the offsetting effects of air near the inlet, at its coolest, being aligned with the fuel inlet. As a consequence, the temperature gradient is smaller in the co-flow case, which must result in a smaller thermal stress in the PEN although the thermal stress distribution was not investigated in this paper.

Fig. 3 illustrates the hydrogen fraction distributions in the co-flow and counter-flow cases. It is obvious that along the direction of fuel flow, the mass fraction of hydrogen on the interface of the electrolyte/anode decreases due to the electrochemical reaction. In particular, for the two flow case, the difference of hydrogen mass fraction is larger in co-flow case, so the utilization of fuel is higher accordingly. With increasing in inlet temperature of

Table 3
The cell operating conditions and parameters used for simulation

Sample number	Fuel			Air		Flow pattern
	Delivery rate (m/s)	Inlet temperature (K)	Hydrogen mass fraction (%)	Delivery rate (m/s)	Inlet temperature (K)	
1	0.5	973	0.8	3	873	Counter-flow Co-flow
2	1.0 0.5	973	0.8	3	873	Counter-flow Co-flow
3	1.0 1.5	973	0.8 0.8	3	873	Co-flow
4	0.5	973	0.9 1	3 3	873	Co-flow
5	0.5	973	0.8	2 1	873	Co-flow

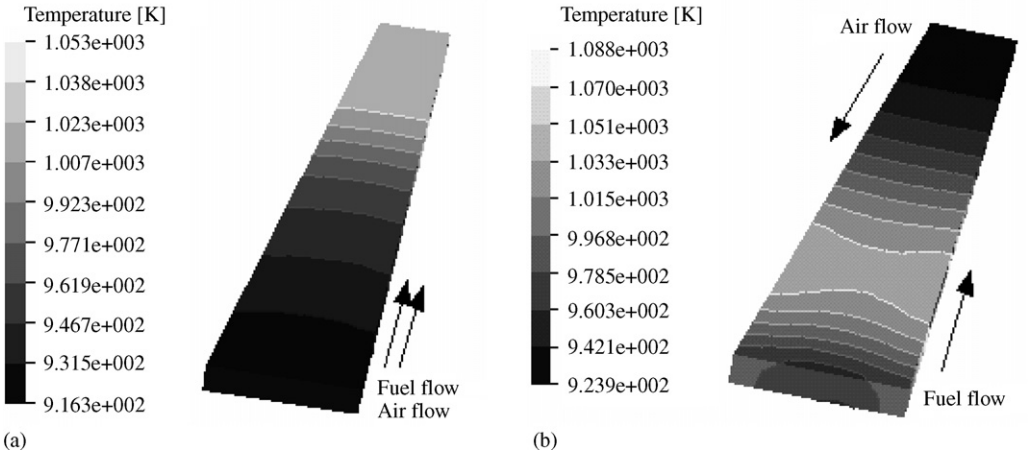

Fig. 2. PEN temperature distributions for the co-flow case (a) and counter-flow case (b) under first working conditions.

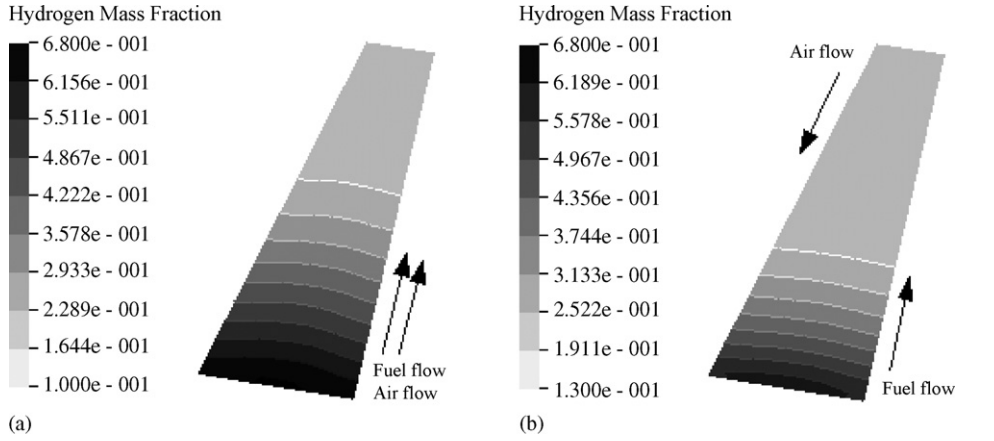

Fig. 3. Hydrogen mass fraction distributions on the interface of anode/electrolyte for the co-flow case (a) and counter-flow case (b) under first working conditions.

the fuel gas, the average temperatures and temperature differences (ΔT) also rise in the two flow cases, as shown in Fig. 4. Consequently, overall considering the temperature distribution and the hydrogen utilization, it is an advantage to choose the co-flow case for SOFC steady operation. For this flow case, other parameters that influence the performance of the SOFC are also studied.

Firstly, we focus on the effects of the fuel gas on the temperature and current density. Fig. 5 shows the PEN temperature and the current density distributions. Increasing the delivery rate of fuel, the average temperature and temperature difference (ΔT) of PEN rise (see Fig. 5(a)), and the average current density also increases (see Fig. 5(b)). This indicates that it is effective for improvement of the electrical performance to increase the

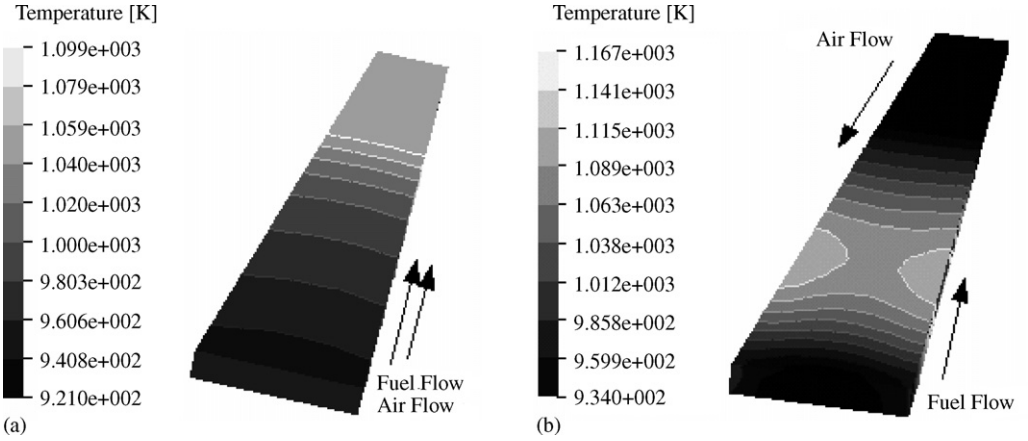

Fig. 4. PEN temperature distributions for the co-flow case (a) and counter-flow case (b) under second working conditions.

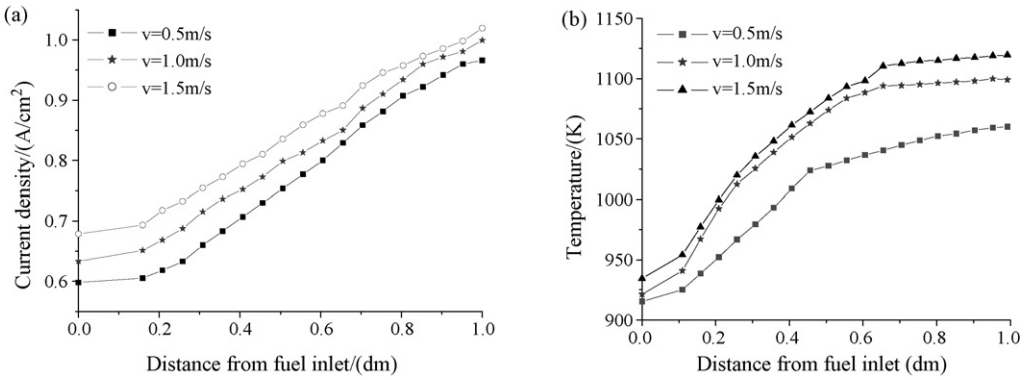

Fig. 5. Current density distributions on the interface of anode/electrolyte (a) and PEN temperature distributions (b) for the co-flow case under third working conditions.

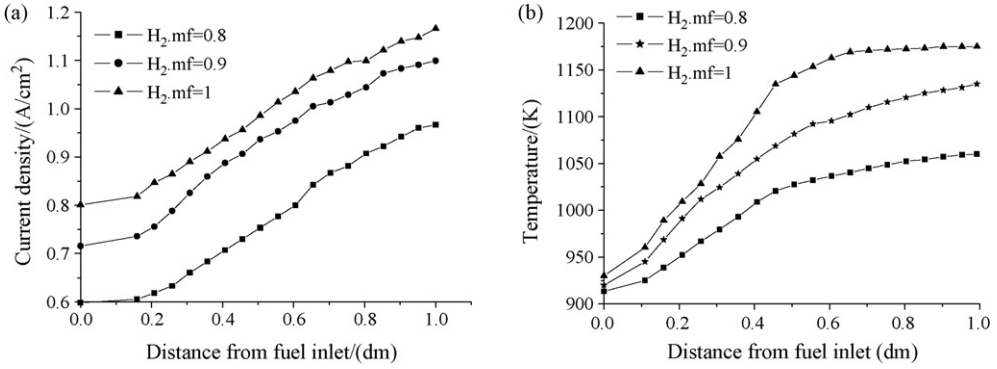

Fig. 6. Current density distributions on the interface of anode/electrolyte (a) and PEN temperature distribution (b) for the co-flow case under forth working conditions.

delivery rate of fuel. But the temperature gradient also rises, which may cause unexpected thermal stresses. Consistent with increasing of the hydrogen proportion from 80 to 90 and 100% in the fuel gas, the average current density, the temperature difference and the average temperature also rise due to the increasing of reaction rate and more reaction heat being accumulated, as shown in Fig. 6.

Figs. 7 and 8 indicate the effects of the fuel on the cell potential. In the anode, the positive active potential directs the transfer current from the catalysts to the electrolyte, and vice versa in the cathode. It can be seen that the absolute value of the active potential in the cathode is higher than that in the anode. Moreover, the active potentials at the anode and the cathode increase from the fuel inlet to the outlet in the co-flow case, and the active potential is highest near the exit of the oxidant flow where it coincides with the regions of lowest oxygen concentration on the cathode. In particular, by increasing the fuel delivery rate and hydrogen mass fraction, the average active potentials at electrodes rise due to the air depletion.

Then the influences of the air flow are also considered. In the SOFC system, air gas not only provides oxygen ions but also has a cooling function. Increasing the inlet velocity of air, the average and maximum temperatures of PEN drop, as shown in Fig. 9, which is because more reaction heat is absorbed and released by the air with the higher delivery rate, although the air utilization is reduced.

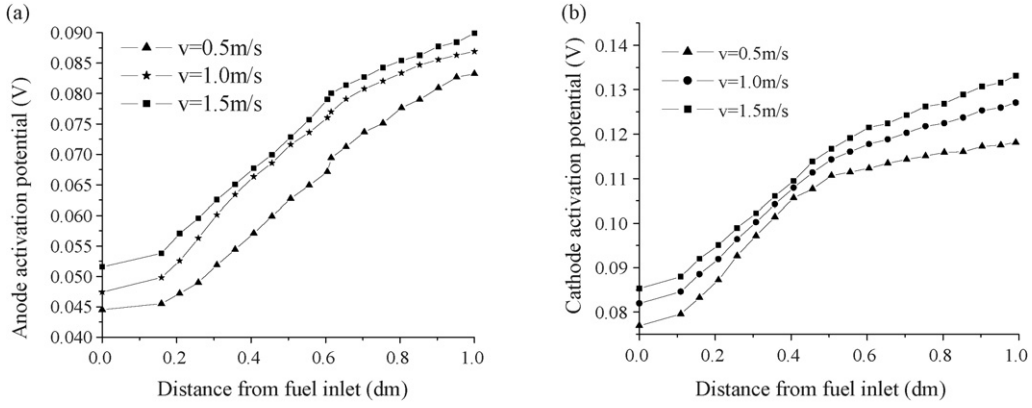

Fig. 7. Activation potential distribution at the anode (a) and cathode (b) for co-flow case under third kind of working conditions.

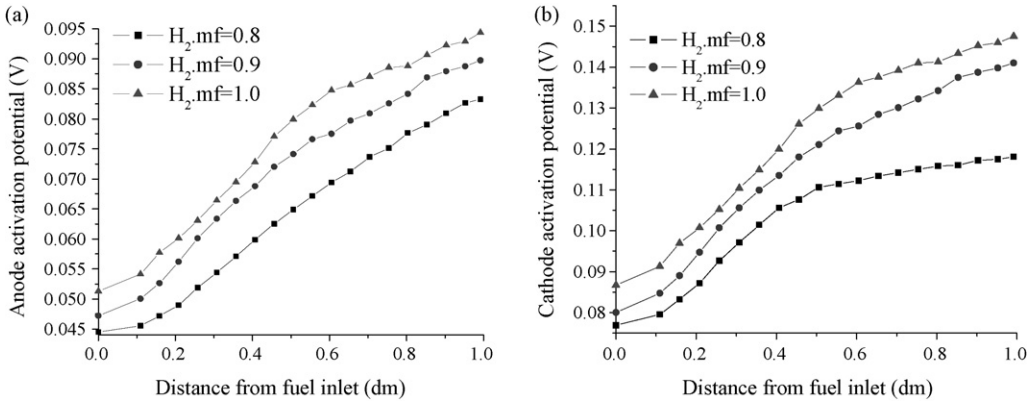

Fig. 8. Activation potential distributions at the anode (a) and cathode (b) for co-flow case under forth working conditions.

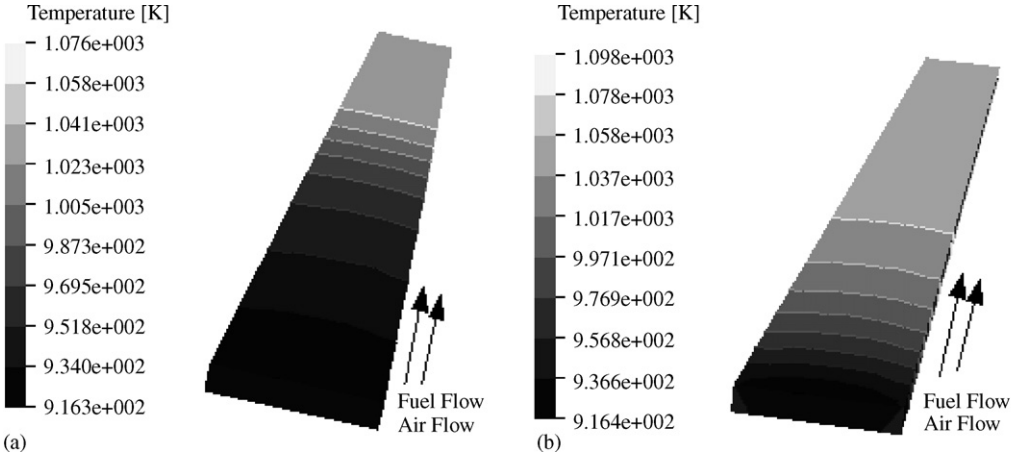

Fig. 9. PEN temperature distributions with air velocity 2 m/s (a) and 1.0 m/s (b) for the co-flow case under fifth working conditions.

Finally, the effects of the anode structure on the concentration potential of SOFC are considered. In this simulation, it is assumed that the electrochemical reactions occur at the interface of electrode and electrolyte. Since the diffusion of reactant from anode channel to the interface of anode/electrolyte is influenced by the thickness and porosity of anode, the concentration potential is also influenced, which must influence the output voltage. Fig. 10 illustrates the variation of the anode concentration potential with the change of anode structure. It is observed that the concentration potential at the anode rises with the anode thickness. However, with the increase of anode porosity, the concentration potential drops.

To validate the numerical simulation for the SOFC performances, some basic tests on the simulative model for the SOFC performances have been carried out, such as complex impedance testing (VMP/2, Princeton Applied Research Corp.,

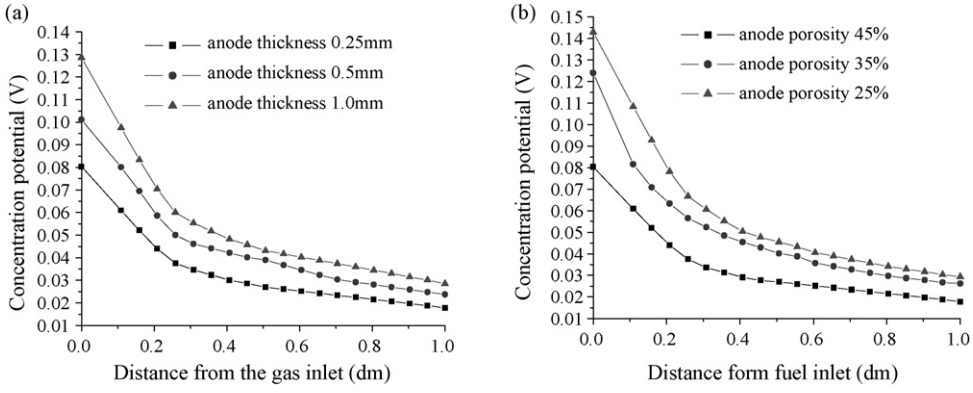

Fig. 10. Concentration potential distributions at the anode with the variation of thickness (a) and porosity (b) of anode for co-flow case under second working conditions.

USA) and testing of the SOFC working performances (SF30, Wuhan Lixing Testing Devices Corp., China). Since the calculation conditions in this paper are different from the testing parameters, the present simulative results cannot be compared with the testing results. However, the present simulative results, such as the temperature distributions and the influence of the flow pattern on the temperature distributions are in qualitative agreement with the results in the reported literature [7,14].

4. Conclusions

The exchange current density was used to couple the thermo-fluid model with the electrochemical model. Source terms were introduced in the governing equations to calculate the mass variation of the reactants and products, and the momentum and energy in the reaction process. In particular, the Darcy law was applied to describe the flow in the porous electrode. The performances of the SOFC in the steady state were simulated and the conclusions were:

(1) The co-flow case, due to its relatively uniform temperature distribution, smaller thermal gradients and higher average current density, offers thermo-structural advantages compared with the counter flow case.
(2) For the co-flow case, with increase in the delivery rate of the fuel gas or hydrogen mass fraction in the fuel, temperature gradients in the PEN and the average current density rise, and the active potentials at the electrodes also rise, which may be harmful to the cell output power . . .. In an attempt to achieve a more uniform temperature distribution, it is effective to decrease the temperature gradients of the PEN by increasing the delivery rate of air.
(3) It is beneficial to decrease the concentration potential of the cell by decreasing the thickness and increasing the porosity of the anode according our simulation results.

Acknowledgements

The authors gratefully acknowledge the contribution of the National Nature Science Foundation of China (NSFC Nos. 50675081 and 50475134).

References

[1] S.C. Singhal, Solid State Ionics 135 (2000) 305–313.
[2] S.C. Singhal, Solid State Ionics 152–153 (2002) 405–410.
[3] L. Yongfeng, D. Xinfa, L. Weiming, Chin. J. Power Sources 6 (2002) 462–465 (in Chinese).
[4] G.Y. Xie, K. Cui, J.Z. Xiao, X.L. Qian, J. HuaZhong Univ. Sci. Technol. 30 (2002) 90–92 (in Chinese).
[5] H. Yakabe, Y. Baba, T. Sakurai, M. Satoh, I. Hirosawa, Y. Yoda, J. Power Sources 131 (2004) 278–284.
[6] K.P. Recknagle, R.E. Williford, L.A. Chick, D.R. Rector, M.A. Khaleel, J. Power Sources 113 (2003) 109–114.
[7] H.W. Zheng, K.S. Ru, X.J. Zhang, Journal of Southwest China Normal University 27 (2002) 789–793 (in Chinese).
[8] M. Iwata, T. Hikosaka, M. Morita, T. Iwanari, K. Ito, K. Onda, Y. Eaaki, Y. Sakaki, S. Nagata, Solid State Ionics 132 (2000) 297–308.
[9] H. Yakabe, T. Ogiwara, M. Hishunuma, I. Yasuda, J. Power Sources 102 (2001) 144–154.
[10] H. Yakabe, T. Sakurai, Solid State Ionics 174 (2004) 295–302.
[11] N. Autissier, D. Larrain, J. Van herle, D. Favrat, J. Power Sources 131 (2004) 313–319.
[12] Y. Shiratori, Y. Yamazaki, J. Power Sources 114 (2003) 80–87.
[13] T. Gen-tu, L. Zhong-yang, N. Ming-jiang, Y. Chun-jiang, C. Ke-fa, Preceeding of CSEE 25 (2005) 116–121 (in Chinese).
[14] S.G. Neophytides, Chem. Eng. Sci. 54 (1999) 4603–4613.
[15] M. Iwata, T. Hikosaka, M. Morita, T. Iwanari, K. Ito, K. Onda, Y. Esaki, Solid State Ionics 132 (2000) 297–308.
[16] H. Jinghuan, Nanjing University of Science Technology (2004) (in Chinese).
[17] L. Ruitai, The Introduction of Heat and Mass Transfer in Porous Material, Scientific Publishing Center, Beijing, PR China, 1995 (in Chinese).
[18] Y. Hui, L. Wenqing, Applied Electrochemical, Scientific Publishing Center, Beijing, PR China, 2001 (in Chinese).
[19] S.H. Chan, K.A. Khor, Z T.A. Xia, J. Power Sources 93 (2001) 130–140.